

Discovery of warm and dense molecular gas surrounding the ring nebula G79.29+0.46

J. R. Rizzo

*Laboratorio de Astrofísica Espacial y Física Fundamental, Apartado 78, E-28691
Villanueva de la Cañada, Spain*

`ricardo.rizzo@laeff.inta.es`

F. M. Jiménez-Esteban

Observatorio Astronómico Nacional, Apartado 112, E-28803 Alcalá de Henares, Spain

`f.jimenez-esteban@oan.es`

and

E. Ortiz

Universidad San Pablo CEU, Urb. Montepríncipe, E-28668 Boadilla del Monte, Spain

`ortiz.eps@ceu.es`

ABSTRACT

We present for the first time the detection of mid- J CO line emission in the outskirts of an evolved massive star, which indicates the presence of warm and/or high density molecular gas. Aiming to learn about the interplay between evolved massive stars and their surroundings, we have carried out CO $J = 2 \rightarrow 1$, $J = 3 \rightarrow 2$, and ^{13}CO $J = 2 \rightarrow 1$ line observations in a $4' \times 4'$ field around the ring nebula G79.29+0.46, which is illuminated by a strong candidate to LBV star. The whole field shows extended predominant emission in both CO and ^{13}CO $J = 2 \rightarrow 1$ lines, which probably comes from the large cloud which contains the star forming region DR 15. When this large-scale emission is removed, minor scales features become evident, particularly in the CO $J = 3 \rightarrow 2$ line, strikingly coincident with the ring nebula. The high critical density of CO $J = 3 \rightarrow 2$ (some 10^4 cm^{-3}) gives additional support for the association with the massive star, since high density molecular gas has more chances to survive in such a harsh environment. This structure may have been produced by the cumulative effect of a strong steady wind in the LBV stage or earlier, which has compressed the

surviving parent molecular cloud. In addition, immersed within this CO feature, we have also discovered a higher density clump (at least several $\sim 10^5 \text{ cm}^{-3}$), unresolved by the telescope and probably having a higher kinetic temperature. Towards the clump, the presence of a jump of $14 - 16 \text{ km s}^{-1}$ in the gas velocity may indicate the existence of a shockfront. This clump may have been created by at least one mass eruption, $10^3 - 10^4 \text{ yr}$ ago. Thus, this work shows that not all the molecular gas is destroyed during massive star evolution, and consequently we are dealing with a new laboratory where one can learn about the mass-loss phenomena associated to the brief LBV stage.

Subject headings: circumstellar matter — ISM: general — ISM: individual (G79.29+0.46) — ISM: molecules — ISM: structure — stars: mass loss

1. Introduction

Massive stars are the most influent sources in the dynamical and chemical evolution of the galactic interstellar medium (ISM). Although relatively few in number, massive stars are the most powerful, the fastest in the evolutionary paths and the richest from a chemical viewpoint. Mass-loss phenomena (strong and dense winds, violent mass ejections) and a very intense UV field provide a significant input to their surroundings, which heats, ionizes, dissociates, blows out, shocks and enriches the ISM as a whole.

According to current evolutionary models (see, for example, Maeder & Meynet 1994; Langer et al. 1994), the main sequence of massive stars lasts several 10^6 yr , while the Wolf-Rayet stage takes some 10^5 yr . All intermediate stages last typically from 10^3 to several 10^4 yr . Stellar winds, size, effective temperature and UV flux vary during each phase by orders of magnitude, while the stellar luminosity remains almost constant. When these changes occur, a number of different structures in the circumstellar/interstellar gas should be produced. Numerical simulations (García-Segura et al. 1996; van Marle et al. 2004) predict the formation of several shockfronts in the ISM at scales from tenths to tens of pc. The possibility of mass eruptions at the intermediate and unstable stages may also add a significant contribution to the nebular mass (Smith & Owocki 2006).

So far, the study of the ISM surrounding massive stars constitutes an excellent method to know about the evolutive history of the exciting source, because it is expected that different evolutive stages would put their “fingerprints” in the circumstellar material. Both neutral and ionized gas have been widely observed in the last decades, and today we can recognize many interstellar bubbles associated to the Main Sequence (Arnal et al. 1999;

Cichowolski et al. 2003) and Wolf-Rayet nebulae (Miller & Chu 1993; Moore et al. 2000), among other galactic structures. In recent years, the hot dust surrounding massive stars was the subject of several near- and mid-IR observational campaigns, and we know about the presence of disks, torus and shells around stars at intermediate evolutive stages (Becklin et al. 1994; O’Hara et al. 2003).

The search for molecular gas in these environments is still limited, possibly due to the *a-priori* hypothesis by which the parent molecular cloud around an evolved massive star may have been destroyed soon after star formation. Even so, the detected low-excitation CO (Marston et al. 1999; Nota et al. 2002; Rizzo et al. 2003a) is giving indications that the molecular component would represent an important contribution to the total mass of gas. Unfortunately, the low- J lines observed to date trace densities as low as few 10^3 cm^{-3} , and the link with the stars or the circumstellar material can only be based on the morphology of the CO structures, and not on any other physical parameter.

A special and motivating case is NGC 2359. To date, this is the only Wolf-Rayet nebula where H_2 has been detected at $2 \mu\text{m}$ (St-Louis et al. 1998). Later, the global distribution of CO has been almost simultaneously mapped using the Kitt Peak (Rizzo et al. 2001a) and SEST radiotelescopes (Cappa et al. 2001), showing an important amount of molecular gas surrounding the optical nebula. Follow-up studies have reported the detection of complex molecules (Rizzo et al. 2001b, 2003b) and multiple layers of rather dense gas ($\simeq 10^4 \text{ cm}^{-3}$; Rizzo et al. 2003c). The origin of the molecular gas seems related to stages previous to Wolf-Rayet (dynamical lifetimes $t_{\text{dyn}} \sim 10^4 - 10^5 \text{ yr}$).

This significant result encourages the search for molecular gas in the environs of evolved massive stars which have not yet become Wolf-Rayet. Of those, the luminous blue variable (LBV) stars are probably the best candidates, due to the “instantaneous” effect of their strong winds and spectacular mass ejections over the star surroundings (Humphreys & Davidson 1994; Nota & Clampin 1997). The nested shells observed in several cases around LBV nebulae span masses from 0.1 to $20 M_{\odot}$, most of which come from short-lived eruptions, such as the well known 19th century outburst of $\eta \text{ Car}$ (Smith & Owocki 2006). The multiple layer structure discovered in NGC 2359, referred above, may have been formed during a previous LBV stage.

A recent census provides a total of 12 confirmed galactic LBV stars and 23 candidates of such objects (Clark et al. 2005). G79.29+0.46 appears as a strong LBV candidate in the sample. Noticed for the first time by Wendker et al. (1991) in a radio map (1420 MHz) of the Cygnus X region, this ringlike structure looks highly symmetric, and has a diameter of $\sim 3'.2$. In a pioneer paper based on continuum and HI observations, Higgs et al. (1994) have shown the thermal nature of the continuum emission, and suggested that the ringlike

nebula is an ionized shell of swept-up interstellar material; in addition, a possible H I bubble is reported at a systemic velocity (LSR) of $\sim -3 \text{ km s}^{-1}$. By assuming a normal gas to dust ratio, the atomic mass is not enough to account for the extinction measured, and hence **a significant amount of molecular gas is predicted**. After examining the IRAS High Resolution images, Waters et al. (1996) concluded that G79.29+0.46 is a detached shell due to an epoch of high mass loss ($\sim 5 \cdot 10^{-4} \text{ M}_{\odot} \text{ yr}^{-1}$), followed by a more quiet period. They have estimated a shell mass of $\sim 14 \text{ M}_{\odot}$, and measured a dust temperature of $60\text{--}77 \text{ K}$. This picture is consistent with the LBV nature of G79.29+0.46’s exciting star, where some different events of mass-loss may have occurred in the recent past.

The central star of G79.29+0.46 has been spectroscopically studied at the optical and the near-infrared wavelengths (Waters et al. 1996; Voors et al. 2000). Its LBV classification is supported by a high luminosity ($> 10^5 \text{ L}_{\odot}$) and a currently high mass-loss rate ($> 10^{-6} \text{ M}_{\odot} \text{ yr}^{-1}$). Its galactic longitude is not adequate to estimate a reliable kinematic distance; even so, Voors et al. (2000) derived a value of $\approx 2 \text{ kpc}$. This is close to 1.7 kpc , the estimated distance to Cygnus OB2 (Massey & Thompson 1991), a huge OB association which G79.29+0.46 may belong to. G79.29+0.46 is behind the Great Cygnus Rift, projected $9'$ to the north-west of the star-forming region DR15, which causes high visual extinction (up to 16 mag ; Knödlseider 2000), and where an important amount of diffuse CO were reported (Schneider et al. 2006, and references therein).

The aim of this work is to detect and to make a first morphological and dynamical analysis of the molecular gas associated to G79.29+0.46. Below we present the results of surveys in the rotational lines of CO $J = 2 \rightarrow 1$ and $3 \rightarrow 2$, and $^{13}\text{CO } J = 2 \rightarrow 1$ surrounding the LBV ring nebula. The obtained results encourage to make further studies about dynamics, excitation and the possible relationship between the molecular gas detected and the ring nebula.

2. Observations

The observations were made with the Submillimeter Telescope (SMT), located on Mount Graham, Arizona. The telescope is a 10.4 m diameter primary with a nutating secondary. Design, optics and structural aspects of the telescope have been extensively described by Baars et al. (1999). The single-polarization receiver SIS-230 was used to observe the CO and $^{13}\text{CO } J = 2 \rightarrow 1$ line emission; on the other hand, the CO $J = 3 \rightarrow 2$ line was observed using the dual-channel SIS-345 receiver. The three lines were mapped in several $\sim 4' \times 4'$ fields around G79.29+0.46, using *on-the-fly* mode, with a fixed position (empty of line emission) as the reference. Several *on-the-fly* maps were later averaged in order to get a final *rms* as

low as possible. The scanning directions and starting positions were different each time to reduce stripping. The Table 1 summarizes some parameters of the observations; for each line, the table indicates the frequency, angular resolution (HPBW), main-beam efficiency and final *rms* of the maps.

The receivers were tuned for double-sideband operation, assuming a sideband ratio of 1 for the system temperature calibration. The receivers were calibrated with ambient-temperature and liquid nitrogen-cooled absorbing loads to determine the receiver noise temperature; calibration of the final data have uncertainties below 20 %. These measurements were made each time a receiver was tuned and at intervals of a few hours thereafter. System temperatures were measured with the standard sky/ambient temperature load method (Kutner & Ulich 1981). Calibrations were performed every 15-20 minutes to track variations in atmospheric opacity. Typical single-sideband system temperatures during the observations were in the range 250 – 400 K for the 1.3 mm lines and 1200 – 2000 K for the 0.8 mm line, depending on the elevation and atmospheric opacity. Two acousto-optic spectrometers (AOS) have been used as backends. The AOS have 2048 channels, and a frequency resolution of 480 kHz, providing a velocity resolution of 0.6 (0.4) km s⁻¹ in the 1.3 mm (0.8 mm) bands, and bandwidths wide enough for galactic emission. The pointing was checked within 2 hr on a planet or other bright continuum source using the integrated line intensity. Corrections to the expected positions for the pointing model were not more than 4'' in either azimuth or elevation. Planet observations were also used to check the main beam efficiency at the observed frequencies, which are also listed in Table 1. Throughout all the paper, the temperatures are on a main-beam scale (T_{MB}), and the velocities refer to the Local Standard of Rest system (V_{LSR}).

3. Results: emission maps around G79.29+0.46

Figure 1 shows a panel of the emission maps corresponding to the CO $J = 2 \rightarrow 1$ line. To provide a first-look morphological comparison with G79.29+0.46, the circle in the center of each map roughly traces the external border of the ring nebula (Higgs et al. 1994). At first sight, we note that large-scale emission dominates all the observed field, mostly at the 2.4 km s⁻¹ map. Despite of this, some minor-scale features can be observed, such as the unresolved arc at the southwest, around ($-80''$, $-110''$). This arc is present in a wide range of velocities, and bounds part of the ring nebula. The inner part of the circle is filled by some low-level emission, especially in the range -3 to +5 km s⁻¹. The emission at the first and last maps do not appear morphologically linked to the ring nebula.

Figure 2 sketches the ¹³CO $J = 2 \rightarrow 1$ emission in a similar fashion to Fig. 1. With the

aim of reducing the map noise, a 2-D hanning filtering has been applied to build the figure. This filtering slightly reduces the angular resolution of the map down to $45''$. In general, the emission of this isotopomer is well correlated with the most intense CO emission in Fig. 1. Similarly, besides the most intense emission at the southeastern corner of the observed field, minor scale feature are also noticed. A systematic deviation of the contours is visible toward the north, north-east, and south-west of the plotted circle. Another outstanding feature of Fig. 2 is the lack of emission in the first, second, and last maps; as this behaviour can not be explained merely by the sensitivity of the map, it clearly indicates that the CO opacity is relatively higher at the central velocities (i.e., in the range -3 to $+10$ km s $^{-1}$), where the isotopic ratio $[\text{CO}]/[^{13}\text{CO}]$ is lower, when compared with the more extreme velocities plotted in Fig. 2.

The emission maps of the CO $J = 3 \rightarrow 2$ line are shown in Fig. 3. Due to a higher velocity resolution, the twelve maps of the figure span the same velocity range as those of Figs. 1 and 2. With the exception of the last map (11.4 km s $^{-1}$), the emission concentrates on the central velocities, mainly on the six central maps. Some extended emission appears at -0.5 and 1.2 km s $^{-1}$, while in the following three maps the CO $J = 3 \rightarrow 2$ emission is concentrated outside the ring nebula. Especially outstanding is again the southwest feature; it has the highest level of the maps (above 10 K on a T_{MB} scale), remains unresolved at 345 GHz, and is widely extended in velocity.

4. Linking the CO to G79.29+0.46: distance, morphology, kinematics

The field of G79.29+0.46 is immersed into Cyg X, a major star-forming region which contains large amounts of molecular gas having densities of some 10^3 cm $^{-3}$ (Schneider et al. 2006). More specifically, G79.29+0.46 is projected close in the sky (only $9'$) to the smaller star-forming region DR 15, although it is not clear if they are physically connected. DR 15 is located at 1.7 ± 0.3 kpc (Schneider et al. 2006). The distance to G79.29+0.46, however, is hard to obtain with similar precision due to the uncertainties in the stellar parameters, dependent on its classification. In this sense, Voors et al. (2000) has made an important contribution, providing a distance in the range 1 to 4 kpc, with a likely value of 2 kpc, close to the distance of DR 15.

Thus, the CO emission presumably linked to G79.29+0.46 are expected to be heavily contaminated by foreground/background emission from DR 15 or Cyg X as a whole. Moreover, contribution from the solar neighbourhood does not have to be disregarded (mostly in the $J = 2 \rightarrow 1$ lines), due to the velocities involved, close to zero. As we have seen in Figs. 1, 2, and 3, most of the CO emission is dominated by large-scale emission which fills all

the mapped area. From a visual inspection to the low resolution maps of Oka et al. (2001), we can relate our large-scale CO emission –which increases towards the southeast– with the molecular cloud around DR 15. Furthermore, in the wide field MSX and SCUBA images of Redman et al. (2003) we can clearly associate the CO emission to the higher column densities of dust. In principle, we can therefore think about the large-scale emission detected in our maps as arising from the foreground/background emission associated to the molecular cloud where DR 15 is embedded.

It is also expected that the CO gas associated to the ring nebula should have minor-scale features, and be morphologically connected to the ring nebula. Thus, in order to propose a link between the observed CO and G79.29+0.46, we should look at the smaller-scale features. In this sense, the southwestern clump is the most prominent feature, visible in all the maps. Other minor scale features can be inferred by the local deviations of the contours already referred to in Sect. 3. In order to better distinguish the local features presumably associated to the ring nebula, we have removed a plane emission (i.e., a polynomial of order 1 in both celestial coordinates) for each velocity channel, in the three observed lines. These planes have been fitted by a least-square method to the whole field, taking the external zone of the field as input, and assuming that every feature outside $\approx 160''$ is purely associated to the foreground/background emission. The results are presented in Fig. 4, where integrated velocity maps in two different velocity ranges ($+1.3$ to $+4.8$ km s $^{-1}$ at panels 4a to 4c; -3.0 to -1.3 km s $^{-1}$ at panels 4d to 4f) are shown for each line. Both the positive and negative velocity ranges have been selected to better show the minor-scale features of the CO emission. The molecular emission is shown by contours, superposed on an ISO 25 μ m-image in grayscale (Trams et al. 1997).

The distribution of the background-subtracted emission is now closely following the ring-shaped geometry of the infrared nebula. At the positive velocity range (Figs. 4a to 4c) the most prominent feature is the southwest clump, clearly visible in both CO lines. The CO $J = 3 \rightarrow 2$ line emission also has lower level contour emission bordering the external part of the nebula. The lack of a ^{13}CO counterpart of the southwestern clump may be due to the background removal method, because the intensity of the local feature may be comparable to the fluctuations of the fitted large-scale plane. Strikingly, at negative velocities (Figs. 4d to 4f), the emission of the three lines closely match the infrared nebula, especially in the western half of the ring. The peak of the emission is again at the southwest, but at an inner position with respect to the southwestern clump at positive velocities.

The morphological coincidence of the small-scale features of the CO emission with the infrared ring nebula encourages their mutual association. At the best of our knowledge, the CO $J = 1 \rightarrow 0$ and $J = 2 \rightarrow 1$ observations presented in AG Car is the only LBV nebula

where a molecular counterpart has been reported (Nota et al. 2002). In that paper, however, no maps were constructed and it is hard to determine if the morphology of the CO resembles or not that found in our data. Moreover, the low- J lines may contain important amounts of diffuse, background or foreground gas. In G79.29+0.46, the small-scale features that more clearly are correlated to the ring nebula are those of the $J = 3 \rightarrow 2$ line (Fig. 4c and 4f), and they are also the most intense. If we also take into account the higher critical density of the $J = 3 \rightarrow 2$ line (some 10^4 cm^{-3}), compared to the low- J lines, we can think about a scenario where high density molecular gas has more chances to survive in harsh environments, dominated by strong and variable stellar winds and UV fields from the massive progenitor star.

The kinematics of the local gas was studied by position-velocity maps across selected strips. On many of them, we could not detect any sign of expansion or rotation of the CO gas. The dominant velocities across the field are from -2 to 0 km s^{-1} , with almost no systematic variations or gradients. This is, on the other hand, the velocity range where most of the low-resolution emission was reported as arising from DR 15 (Oka et al. 2001). An outstanding exception to this general trend is shown in Fig. 5. This figure was constructed by selecting the strip indicated in Fig. 4c, along a northeast to southwest direction (exactly 45° from north to east). The slice was selected to pass through the southwest arc (at $\sim 260''$ in Fig. 5), where a sudden broadening occurs. This broadening grows up to 14 km s^{-1} (from -2 to $+12 \text{ km s}^{-1}$), and is limited to an angular extension comparable to the beamsize. It is also noticeable that the CO velocity shifts when the strip passes from the inner to the outer region of the nebula, i.e., when passes through the southwest arc.

The feature displayed in Fig. 5 is a dynamical indicator of a low-velocity shock, acting beyond the ionized ring nebula at a projected velocity of 14 km s^{-1} . This assumption is supported by two facts: firstly, the region affected by the broadening is relatively thin, because it is unresolved by our beam; and secondly, there is no smooth variations of the velocity between the inner and the outer regions. An important, additional argument is provided by the fact that there is no CO emission arising from DR 15 or other close objects, above 10 km s^{-1} ; in this sense, the Fig. 4c of Oka et al. (2001) is eloquent, showing no features at velocities above 10 km s^{-1} . In other words, the CO velocity outside the ring nebula is locally exceptional, and it may only be explained by some kind of interaction with the LBV-candidate star. The presence of shocked gas close to the hot star encourages its association and explains its own existence, because the (relatively) recent mass eruptions and variable winds after the main sequence may have produced some sort of features like the ones recognized in the molecular circumstellar gas.

As were mentioned in the introduction, an increasing number of hydrodynamical sim-

ulations are predicting the presence of several shocks in the environs of evolved massive stars (García-Segura et al. 1996; van Marle et al. 2004). This shocked region is certainly of particular interest, because it may constitute a good laboratory to test these theoretical predictions. This is especially true when we take into account the multiple layers reported by Rizzo et al. (2003c) surrounding a Wolf-Rayet nebula (NGC 2359), where a previous LBV stage was assigned as the responsible of such layers. The chemistry of the molecular gas in the southwestern clump may also be of particular interest, with a scenario characterized by a shocked cloud, and close to a highly-obscured, hot, and evolved star.

The velocity range of the unshocked CO (from -3 to $+1$ km s $^{-1}$) is –within the uncertainties of the observations and the expected dispersion– coincident with the H I hole’s systemic velocity reported by Higgs et al. (1994). This H I counterpart may represent the main sequence signature of the star progenitor, as in many other cases of the Galaxy (see, for example, Arnal et al. 1999; Rizzo et al. 2001a; Cichowolski et al. 2003). These velocities do not differ too much to those of the metal lines (Voors et al. 2000) and Br α (Waters et al. 1996) from the star ¹.

Below we discuss the particular physical conditions of the molecular gas linked to G79.29+0.46, and also provide some quantitative arguments about its possible origin.

5. Discussion

5.1. Physical parameters: the LVG approach

As we mentioned in the earlier sub-section, the detected molecular gas should have physical conditions which are different to those of the general ISM. The detected CO may simply be interstellar gas accumulated by the stellar wind, the results of several ejecta, or the relics of the parent molecular cloud, affected by the destructive action of UV radiation and/or pushing wind. An estimate of the molecular mass, together with the neutral atomic and the ionized gas masses, may complete the energetic balance related to the mechanical input from the exciting star. Other local parameters, such as the gas temperature or the density, will help to better describe the physical conditions in the studied region.

In a wide variety of galactic scenarios, CO was found to be close to LTE but having a high opacity (Lequeux 2005). From the most common values of the CO to ^{13}CO $J = 2 \rightarrow 1$

¹Note that, in both papers, the conversion from heliocentric to LSR reference systems were made in the wrong sense, and consequently the star and nebular velocities result to be ~ 34 km s $^{-1}$ higher than the published ones.

line ratio (between 3 and 5 when ^{13}CO is detected) we confirm that both CO lines are optically thick. Furthermore, the high intensity of the CO $J = 3 \rightarrow 2$ line (comparable or even higher than the $J = 2 \rightarrow 1$ line), indicates that we are dealing with densities ($n(\text{H}_2)$) above 10^4 cm^{-3} , and rotational temperatures (T_{rot}) of 40 K or more.

We can make a first approach to the physical conditions of the CO by using a LVG code to predict the observed intensities and line ratios. In order to compare the LVG modelling with the observations, we have used the line-integrated maps already shown in Fig. 4 in the two velocity intervals. The CO $J = 3 \rightarrow 2$ map has been convolved to the $J = 2 \rightarrow 1$ angular resolution to work with a directly comparable T_{MB} scale. The CO to ^{13}CO $J = 2 \rightarrow 1$ line ratio varies from 2 to 8, while the CO $J = 3 \rightarrow 2$ to $2 \rightarrow 1$ line ratio (hereafter referred to as R_{exc}) varies from 0.3 to 1.7 on a T_{MB} scale in both velocity intervals.

After analyzing the emission in all the lines, as well as the line ratios, we have proceeded with the LVG modelling by choosing characteristic regions within the observed field. These regions are indicated in Fig. 6, and the meanings are as follows:

Region A: It contains the most intense emission from the southwestern clump in the (1.3, 4.8) km s^{-1} velocity interval. This region may have representative values for both the total mass and $n(\text{H}_2)$ of the emission at positive velocities.

Region B: This region corresponds to the maximum R_{exc} in both velocity intervals, and points out the maximum densities expected in the whole area.

Region C: This region comprises most of the emission at negative velocities (excluding region B), coincident with the ring nebula. It may represent the most common physical conditions in the velocity interval (-3, -1.3) km s^{-1} , and may contain most of the mass.

Region D: This is a control region, with no significant features associated to the ring nebula. This is built just to compare the results of LVG modelling with the other regions, and to check the validity of the method.

The four regions defined are sketched in Fig. 6 superposed to the distribution of R_{exc} in the (1.3, 4.8) km s^{-1} velocity interval in greyscale, and to some contours of the CO $J = 3 \rightarrow 2$ emission in both velocity intervals (see caption). Note that greyscale peaks at region B and not at region A, where the line intensity is higher for positive velocities. Qualitatively, region B might have a higher density but lower mass than the region A, where we have found the CO absolute peak and a high (but not the highest) R_{exc} .

We have modelled the CO emission for different values of the kinetic temperature (T_{k}), namely 40, 70, and 100 K. For a given T_{k} , we have used the ^{13}CO $J = 2 \rightarrow 1$ line intensity and R_{exc} as input, and thus predicted the ^{13}CO column density ($N(^{13}\text{CO})$) and $n(\text{H}_2)$.

According to the method, $N(^{13}\text{CO})$ is most sensitive to the line intensity, and does not vary too much with T_k (Lequeux 2005). The obtained values for $N(^{13}\text{CO})$ and $n(\text{H}_2)$ were later introduced to obtain the line opacities and excitation temperatures. The CO column density ($N(\text{CO})$) was obtained from $N(^{13}\text{CO})$ by assuming a CO to ^{13}CO relative abundance of 70 (Wilson & Matteucci 1992). Finally, the total molecular mass was derived from $N(\text{CO})$, by assuming a CO abundance of $8 \cdot 10^{-5}$, a distance of 1.7 kpc, and including the correction for the presence of He and other elements. The results from the LVG modelling are summarized in Table 2. For each velocity interval, we have indicated the region, its angular size, the assumed T_k , and the obtained values for $n(\text{H}_2)$, $N(\text{CO})$, and the total molecular mass. Finally, the last column provided a brief description of each region.

The visual absorption A_V measured towards G79.29+0.46 varies from 12 (Trams et al. 1999) to 15 mag (Voors et al. 2000). By assuming a crude gas-to-dust ratio of

$$N(\text{HI}) + 2 N(\text{H}_2) \sim 10^{21} A_V$$

we derive $N(\text{H}_2) \leq 6 - 7.5 \cdot 10^{21} \text{ cm}^{-2}$. For a normal CO abundance ($8 \cdot 10^{-5}$), a general $N(\text{CO})$ value of $\leq 5 - 6 \cdot 10^{17} \text{ cm}^{-2}$ is expected. The values of $N(\text{CO})$ obtained in our control regions are one order of magnitude lower, which may indicate that most of the local gas is in atomic phase (both neutral and ionized). Moreover, the densities of the control regions are the lowest of the table, which again reinforces the proposed link of the molecular gas characterized by the regions A, B, and C. While the densities of region D are around 10^3 cm^{-3} , the values for the other regions show an enhancement of one or two orders of magnitude.

The total mass at positive velocities rounds $8 M_\odot$, roughly distributed between clumps A ($5 M_\odot$) and B ($3 M_\odot$). At negative velocities, a total mass of $5 M_\odot$ is computed, distributed between the clump B ($1.5 M_\odot$) and the northwestern arc ($3.5 M_\odot$). The missing mass of the method, mostly due to the reduction of the velocity intervals and to the selected regions, is in any case lower than $2 M_\odot$. These masses fall within the range of those expected in LBV outbursts (Smith & Owocki 2006), and to other verified mass eruptions like in η Carina (Smith et al. 2003), or P Cyg (Meaburn 2001). Although the lack of symmetry of the associated CO is puzzling, the hypothesis of mass ejections as the origin of such structures is worth to be considered in the future. A follow-up study should be carried out to observe other emission lines at higher frequencies or larger telescopes, capable of resolving the southwestern structure. The dominant physical processes may also be inferred by getting information from molecular tracers of shocks and PDRs.

The assumed T_k is surely not uniform along the whole field: probably, the emission at negative velocities is better described by higher T_k than the regions emitting at positive velocities. As expected, the column densities are almost independent from T_k , and the

variations are well below the observational uncertainties. The $^{13}\text{CO } J = 2 \rightarrow 1$ line was found to be optically thin in all cases. However, both CO lines are optically thick; the $J = 3 \rightarrow 2$ line systematically has a larger opacity than the $J = 2 \rightarrow 1$ line, which may result in larger values of R_{exc} , and consequently $n(\text{H}_2)$. The $^{13}\text{CO } J = 2 \rightarrow 1$ line is subthermally excited in all cases. For positive velocities, the LVG modelling needs an excitation temperature above 40 K, indicating a T_{k} well above such value. In fact, fitting was impossible in region B for $T_{\text{k}} = 40$ K.

5.2. On the origin of the detected molecular gas

The high densities found in the field, particularly in the regions A and B, strengthen the hypothesis of several shockfronts acting upon the circumstellar medium around G79.29+0.46. A set of shockfronts is the natural consequence of the presence of different wind regimes during star evolution, and the probable occurrence of mass eruptions (García-Segura et al. 1996; van Marle et al. 2004). So far, it is important to associate the different features with specific evolutive stages of the star progenitor.

We can deal with a rough estimate of the age of the high-density gas, by taking into account the morphology and kinematics presented above. For an assumed distance of 1.7 kpc, the southwestern clump is projected at a distance of ~ 1 pc. A lower limit for the shock velocity would be 14 km s^{-1} , the magnitude of the “jump” in Fig. 5. By adopting these values, a crude estimate of the dynamical time would be

$$t_{\text{dyn}} < \frac{R}{V_{\text{shock}}} = \frac{1 \text{ pc}}{14 \text{ km s}^{-1}} \simeq 7 \times 10^4 \text{ yr.}$$

This value of t_{dyn} should be regarded as a loose upper limit for the age of the shock, mainly due to the fact that: (i) the present shock velocity may be higher than 14 km s^{-1} , because this is the most conservative value, and just a radial projection of the real shock velocity; (ii) the shock might have started with values of several hundreds of km s^{-1} , and then have been decelerated when travelling into the circumstellar gas. If this were the case, the real age would be one order of magnitude lower. By looking at the high regularity of the torus-like nebula, a reasonable value for the age of the structure may be below 10^4 yr, perhaps some 10^3 yr.

The youth of this structure allows us to associate the molecular shockfront with the actual LBV phase, which might have experienced several episodes of mass ejection in the near past. As the material is indeed more disperse than, for example, η Carina, we can speculate about two possibilities: (i) G79.29+0.46 is older than η Carina, and hence has had more time to disperse its surroundings; or (ii) the energy involved in G79.29+0.46 is

greater than in η Carina. The first hypothesis seems more plausible, because of the size of the circumstellar material associated to G79.29+0.46, and because recent, violent eruptions of η Carina have been recorded in the 19th century. Even so, it is interesting to explore both possibilities, as well as to go deep into a comparison of both objects, in order to shed some light on the interplay between these type of stars and their outskirts.

6. Conclusions

A region of $4' \times 4'$ in the field of the ring nebula G79.29+0.46 has been mapped in the CO $J = 2 \rightarrow 1$ and $3 \rightarrow 2$, and the ^{13}CO $J = 2 \rightarrow 1$ emission lines, with a maximum angular resolution of $24''$, equivalent to ~ 0.2 pc at an assumed distance of 1.7 kpc. We report for the first time the detection of a mid- J CO emission line from the surroundings of a LBV nebula. Provided the excitation conditions of the CO $J = 3 \rightarrow 2$ line, the studied gas is presumably warm (more than 33 K) and dense (above some 10^4 cm^{-3}). As a first result of this work, it is shown that not all the molecular gas is destroyed during massive star evolution, and consequently we are dealing with a new laboratory where one can learn about the mass-loss phenomena associated to the brief LBV stage.

The CO emission is dominated by large scale features, which uniformly increases towards the southeast; this background/foreground emission is probably associated to DR 15, due to its close location and the velocity range of emission. Minor scale features, however, show a morphology completely different, dominated by a large arc which coincides with more than half of the infrared ring nebula, and bounding it at a projected distance of up to 1 pc. This emission is particularly intense (in the $J = 3 \rightarrow 2$ line) towards the southwest, where a more conspicuous zone is embedded. Moreover, there is a shockfront of a projected velocity of 14 km s^{-1} acting precisely in this southwestern clump.

We have predicted the observed line emission by LVG modelling. A minimum T_k of 40 K was determined in an extended area which have densities of the order of 10^4 cm^{-3} . Immersed within this plateau, there are two outstanding clumps (regions A and B), which have densities well above 10^5 cm^{-3} and probably a higher T_k .

The total molecular mass associated to the nebula is ~ 13 to $15 M_\odot$, while the clump masses are about $5 M_\odot$ each. Most of the gas may result from the surviving parent molecular cloud, later compressed by steady stellar winds and radiation pressure. The origin of the clumps may be different, and we can not rule out the existence of recent mass eruptions. The higher density, the presence of a shockfront and the mass involved may be indicators of violent events, produced $\sim 10^4$ yr ago, or less. This fact, together with the high symmetry

of the nebula, points to an LBV origin of the feature.

This study of the molecular component directly associated to the LBV stage may help to understand the recent past of G79.29+0.46, and therefore the evolutive mechanisms of this kind of objects. So far, it is worth making more observational efforts in order to resolve the emission, particularly in the clump. The differences between regions A and B are puzzling, and may indicate the existence of more than one mass eruption in the recent past of the progenitor of G79.29+0.46. A follow-up study of complex molecules should also be carried out, because they can provide information about the physical parameters in detail. The chemistry of the molecular gas in this region may also be of particular interest, with a scenario characterized by a shocked cloud, and close to a highly-obscured, hot, and evolved star. An abundance study of such molecules may point to the dominant emission mechanisms in the zone, which can be related to the ionized and atomic neutral gas, together with the hot circumstellar dust. Finally, other surveys of CO emission in LBVs and other evolved massive stars will also help to understand how frequent the mass eruptions are in this class of objects, and how important they are when compared to the steady high mass loss and to the UV destructive radiation.

We are grateful to the technical staff of SMT for their kind assistance during both the remote and on-site observations. We also wish to acknowledge the anonymous referee by his/her useful comments, which greatly improved the paper. Data reduction and analysis were done using the GILDAS package (<http://www.iram.fr/IRAMFR/GILDAS>). This work is supported by the Spanish Ministerio de Ciencia y Técnica, through grant AYA2003-06473. The SMT is operated by the Arizona Radio Observatory (ARO), Steward Observatory, University of Arizona.

Facilities: ARO(SMT).

REFERENCES

- Arnal, E. M., Cappa, C. E., Rizzo, J. R., & Cichowolski, S. 1999, *AJ*, 118, 1798
- Baars, J. W. M., Martin, R. N., Mangum, J. G., McMullin, J. P., & Peters, W. L. 1999, *PASP*, 111, 627
- Becklin, E. E., Zuckerman, B., McLean, I. S., & Geballe, T. R. 1994, *ApJ*, 430, 774
- Cappa, C. E., Rubio, M., & Goss, W. M. 2001, *AJ*, 121, 2664
- Cichowolski, S., Arnal, E. M., Cappa, C. E., Pineault, S., & St-Louis, N. 2003, *MNRAS*, 343, 47
- Clark, J. S., Larionov, V. M., & Arkharov, A. 2005, *A&A*, 435, 239
- García-Segura, G., Mac Low, M.-M., Langer, N. 1996, *A&A*, 305, 229
- Higgs, L. A., Wendker, H. J., & Landecker, T. L. 1994, *A&A*, 291, 295
- Humphreys, R. M., & Davidson, K. 1994, *PASP*, 106, 1025
- Knödlseeder, J. 2000, *A&A*, 360, 539
- Kutner, M. L., & Ulich, B. L. 1981, *ApJ*, 250, 341
- Langer, N., Hamann, W.-R., Lennon, M., Najarro, F., Pauldrach, A. W. A., & Puls, J. 1994, *A&A*, 290, 819
- Lequeux, J. 2005, *The interstellar medium. Astronomy and astrophysics library*, Berlin: Springer, 2005
- Maeder, A., & Meynet, G. 1994, *A&A*, 287, 803
- Marston, A. P., Welzmler, J., Bransford, M. A., Black, J. H., & Bergman, P. 1999, *ApJ*, 518, 769
- Massey, P., & Thompson, A. B. 1991, *AJ*, 101, 1408
- Meaburn, J. 2001, *ASP Conf. Ser. 233: P Cygni 2000: 400 Years of Progress*, 233, 253
- Miller, G. J., & Chu, Y.-H. 1993, *ApJS*, 85, 137
- Moore, B. D., Hester, J. J., & Scowen, P. A. 2000, *AJ*, 119, 2991

- Nota, A., & Clampin, M. 1997, ASP Conf. Ser. 120: Luminous Blue Variables: Massive Stars in Transition, 120, 303
- Nota, A., Pasquali, A., Marston, A. P., Lamers, H. J. G. L. M., Clampin, M., & Schulte-Ladbeck, R. E. 2002, AJ, 124, 2920
- O’Hara, T. B., Meixner, M., Speck, A. K., Ueta, T., & Bobrowsky, M. 2003, ApJ, 598, 1255
- Oka, T., et al. 2001, ApJ, 558, 176
- Redman, R. O., Feldman, P. A., Wyrowski, F., Côté, S., Carey, S. J., & Egan, M. P. 2003, ApJ, 586, 1127
- Rizzo, J. R., Martín-Pintado, J., & Mangum, J. G. 2001a, A&A, 366, 146
- Rizzo, J. R., Martín-Pintado, J., & Henkel, C. 2001b, ApJ, 553, L181
- Rizzo, J. R., Martín-Pintado, J., & Desmurs, J.-F. 2003a, IAU Symposium, 212, 740
- Rizzo, J. R., Martín-Pintado, J., & Desmurs, J.-F. 2003b, IAU Symposium, 212, 742
- Rizzo, J. R., Martín-Pintado, J., & Desmurs, J.-F. 2003c, A&A, 411, 465
- Schneider, N., Bontemps, S., Simon, R., Jakob, H., Motte, F., Miller, M., Kramer, C., & Stutzki, J. 2006, A&A, 458, 855
- Smith, N., Gehrz, R. D., Hinz, P. M., Hoffmann, W. F., Hora, J. L., Mamajek, E. E., & Meyer, M. R. 2003, AJ, 125, 1458
- Smith, N., & Owocki, S. P. 2006, ApJ, 645, L45
- St-Louis, N., Doyon, R., Chagnon, F., & Nadeau, D. 1998, AJ, 115, 2475
- Trams, N. R., Voors, R. H. M., & Waters, L. B. F. M. 1997, Ap&SS, 255, 195
- Trams, N. R., van Tuyll, C. I., Voors, R. H. M., de Koter, A., Waters, L. B. F. M., & Morris, P. W. 1999, LNP Vol. 523: IAU Colloq. 169: Variable and Non-spherical Stellar Winds in Luminous Hot Stars, 523, 71
- van Marle, A. J., Langer, N., & García-Segura, G. 2004, RMA&A Conf. Ser., 22, 136
- Voors, R. H. M., Geballe, T. R., Waters, L. B. F. M., Najarro, F., & Lamers, H. J. G. L. M. 2000, A&A, 362, 236

- Waters, L. B. F. M., Izumiura, H., Zaal, P. A., Geballe, T. R., Kester, D. J. M., & Bontekoe, T. R. 1996, *A&A*, 313, 866
- Wendker, H. J., Higgs, L. A., & Landecker, T. L. 1991, *A&A*, 241, 551
- Wilson, T. L., & Matteucci, F. 1992, *A&A Rev.*, 4, 1

Table 1. Observational parameters

line	frequency (GHz)	HPBW (")	η_{MB}	rms^{a} (K)
CO $J = 2 \rightarrow 1$	230.5380000	36	0.85	0.4
^{13}CO $J = 2 \rightarrow 1$	220.3986765	38	0.86	0.2
CO $J = 3 \rightarrow 2$	345.7959899	24	0.60	0.6

^aApproximate rms of the final maps, in T_{R}^* scale

Table 2. Physical parameters in selected regions

Region	Area (ster)	T_{k} (K)	$n(\text{H}_2)$ (cm^{-3})	$N(\text{CO})$ (cm^{-2})	Mass (M_{\odot})	Description
Positive velocities: from 1.3 to 4.8 km s ⁻¹ :						
A	$5.5 \cdot 10^{-8}$	40	$2.4 \cdot 10^5$	$1.4 \cdot 10^{17}$	5.2	Southwestern clump.
		70	$1.7 \cdot 10^4$	$1.2 \cdot 10^{17}$	4.5	CO $J = 3 \rightarrow 2$ peak.
		100	$9.1 \cdot 10^3$	$1.2 \cdot 10^{17}$	4.5	
B	$3.9 \cdot 10^{-8}$	40	$> 4 \cdot 10^6$	$8.3 \cdot 10^{16}$	2.7	R_{exc} peak.
		70	$1.3 \cdot 10^5$	$9.5 \cdot 10^{16}$	3.1	
		100	$2.0 \cdot 10^4$	$8.2 \cdot 10^{16}$	2.7	
D	$7.6 \cdot 10^{-8}$	40	$7.7 \cdot 10^3$	$5.1 \cdot 10^{16}$	2.5	“Control” region.
		70	$4.1 \cdot 10^3$	$5.0 \cdot 10^{16}$	2.5	
		100	$2.5 \cdot 10^3$	$4.9 \cdot 10^{16}$	2.4	
Negative velocities: from -3.0 to -1.3 km s ⁻¹ :						
B	$3.9 \cdot 10^{-8}$	40	$2.7 \cdot 10^4$	$4.7 \cdot 10^{16}$	1.6	CO $J = 3 \rightarrow 2$ and
		70	$8.8 \cdot 10^3$	$4.5 \cdot 10^{16}$	1.5	R_{exc} peaks.
		100	$6.4 \cdot 10^3$	$4.6 \cdot 10^{16}$	1.5	
C	$4.0 \cdot 10^{-7}$	40	$1.7 \cdot 10^4$	$1.3 \cdot 10^{16}$	3.4	Most extended
		70	$6.5 \cdot 10^3$	$1.3 \cdot 10^{16}$	3.4	emission, coincident
		100	$4.8 \cdot 10^3$	$1.3 \cdot 10^{16}$	3.5	with ring nebula.
D	$7.6 \cdot 10^{-8}$	40	$6.4 \cdot 10^3$	$2.7 \cdot 10^{16}$	1.3	“Control” region.
		70	$3.2 \cdot 10^3$	$2.6 \cdot 10^{16}$	1.2	
		100	$2.2 \cdot 10^3$	$2.6 \cdot 10^{16}$	1.2	

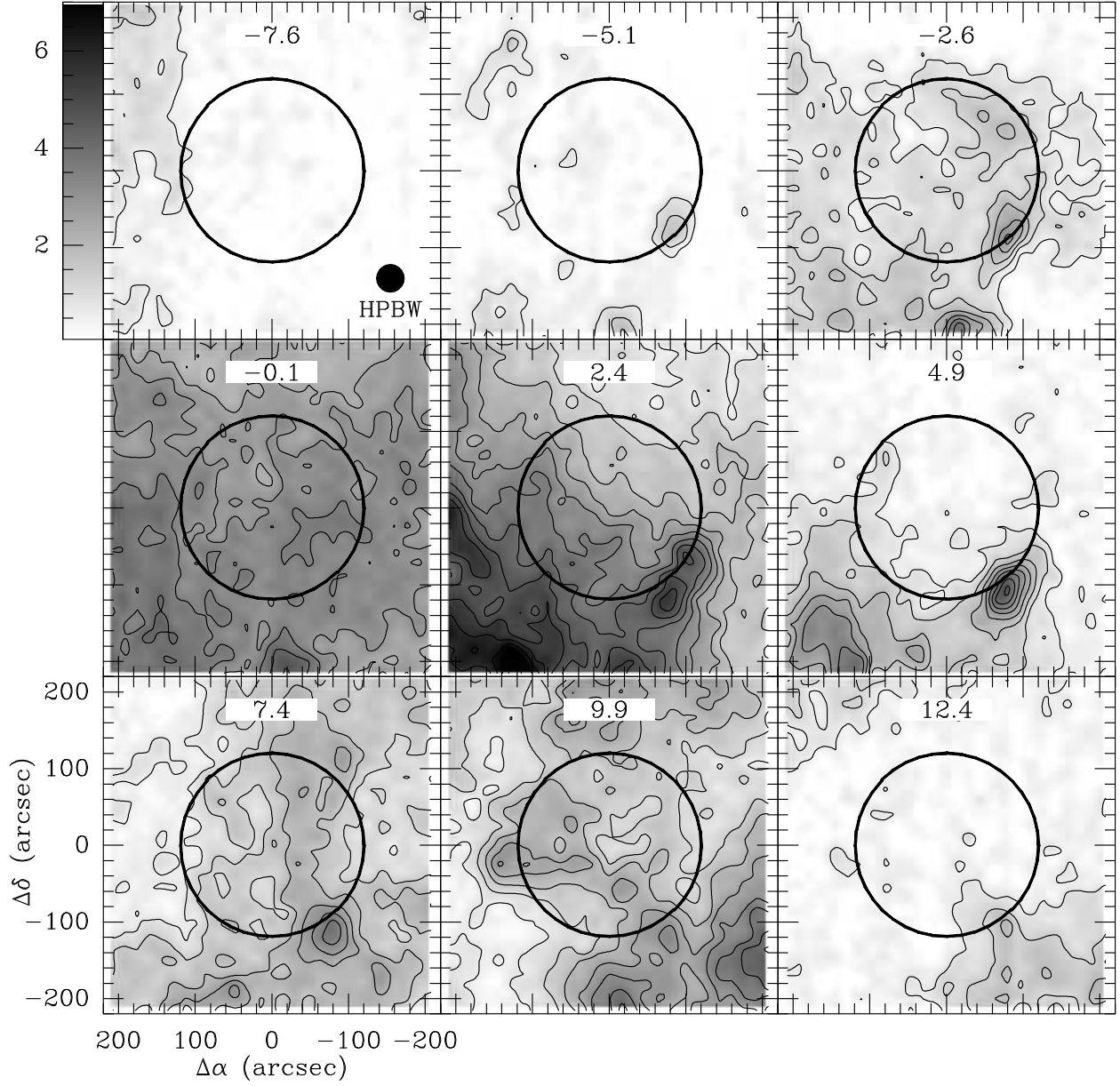


Fig. 1.— CO $J = 2 \rightarrow 1$ emission maps in the field of G79.29+0.46. Central velocities (in km s^{-1}) are indicated on top of each map, and correspond to the mean of two consecutive channels. Starting and spacing contours are 0.6 K (in T_{MB} scale). Greyscale (in K) and beam size are indicated in the top left map. The central circle, $\sim 4'$ in diameter, roughly sketches the external border of the ring nebula. Equatorial coordinates (J2000.0) are offsets from the exciting star of G79.29+0.46

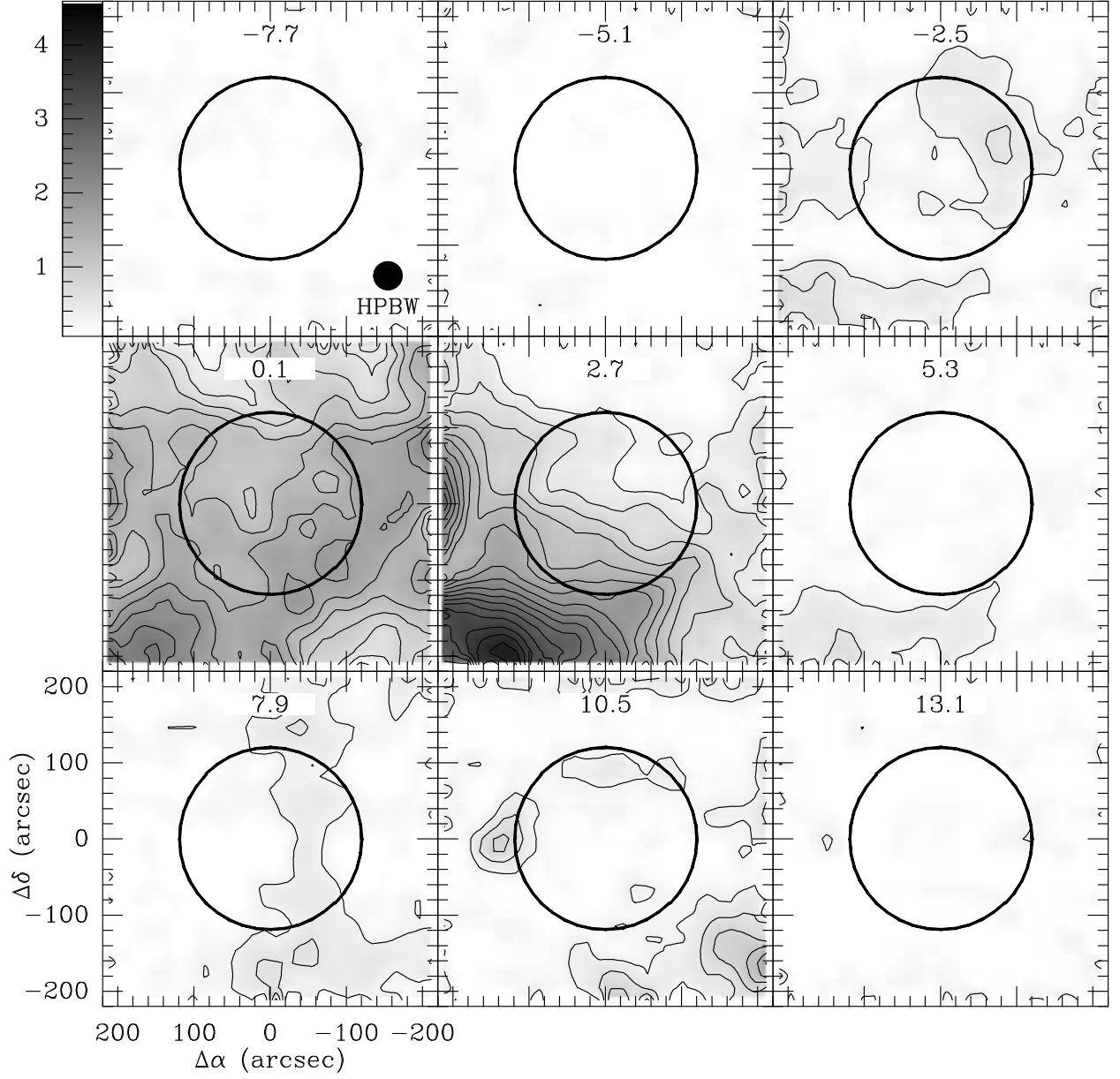


Fig. 2.— The same as for Fig. 1, but for the $^{13}\text{CO } J=2 \rightarrow 1$ line. Starting and spacing contours are 0.25 K

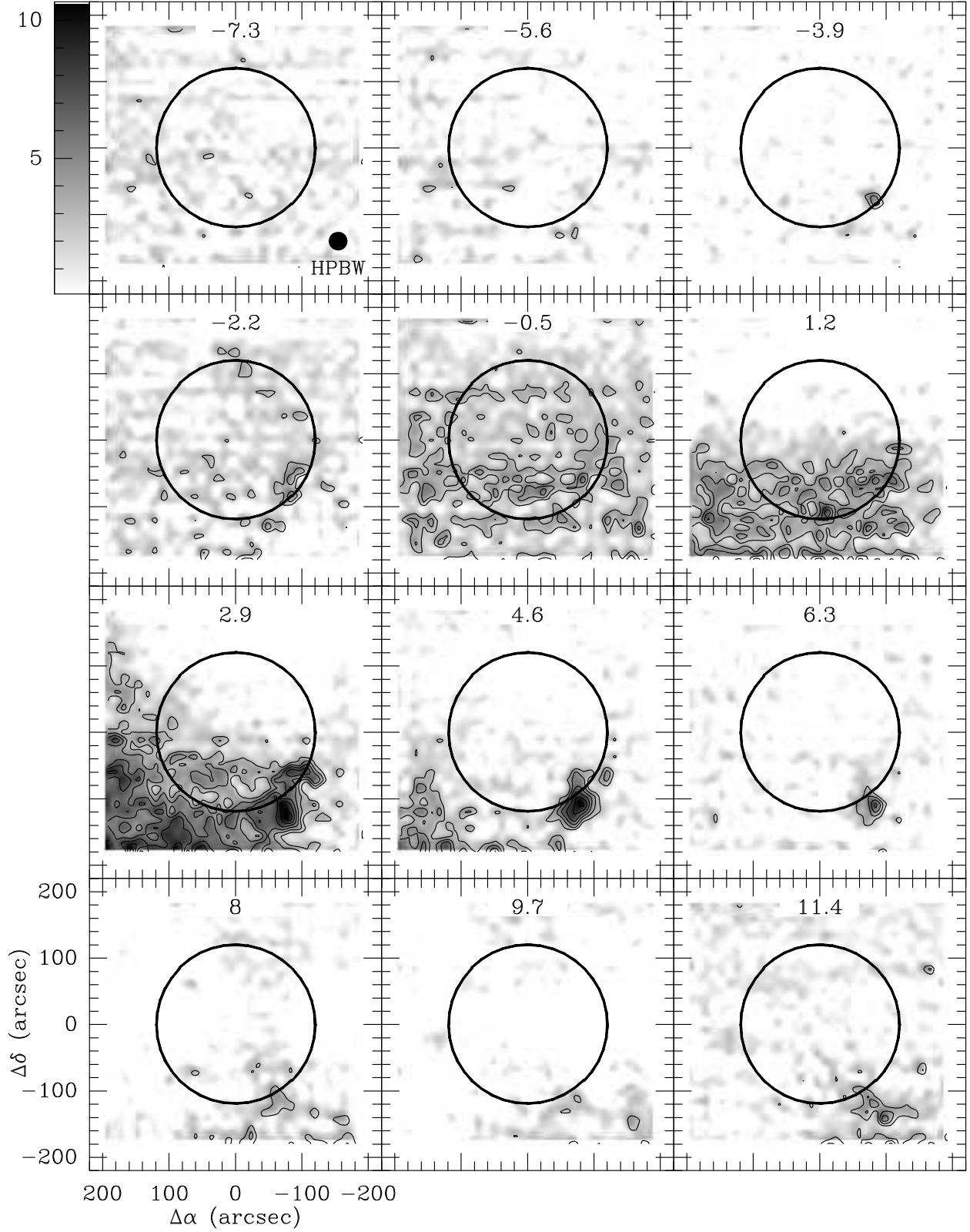


Fig. 3.— The same as for Figs. 1 and 2, but for the CO $J = 3 \rightarrow 2$ line. Contours are spaced by 1.5 K, starting in 3 K

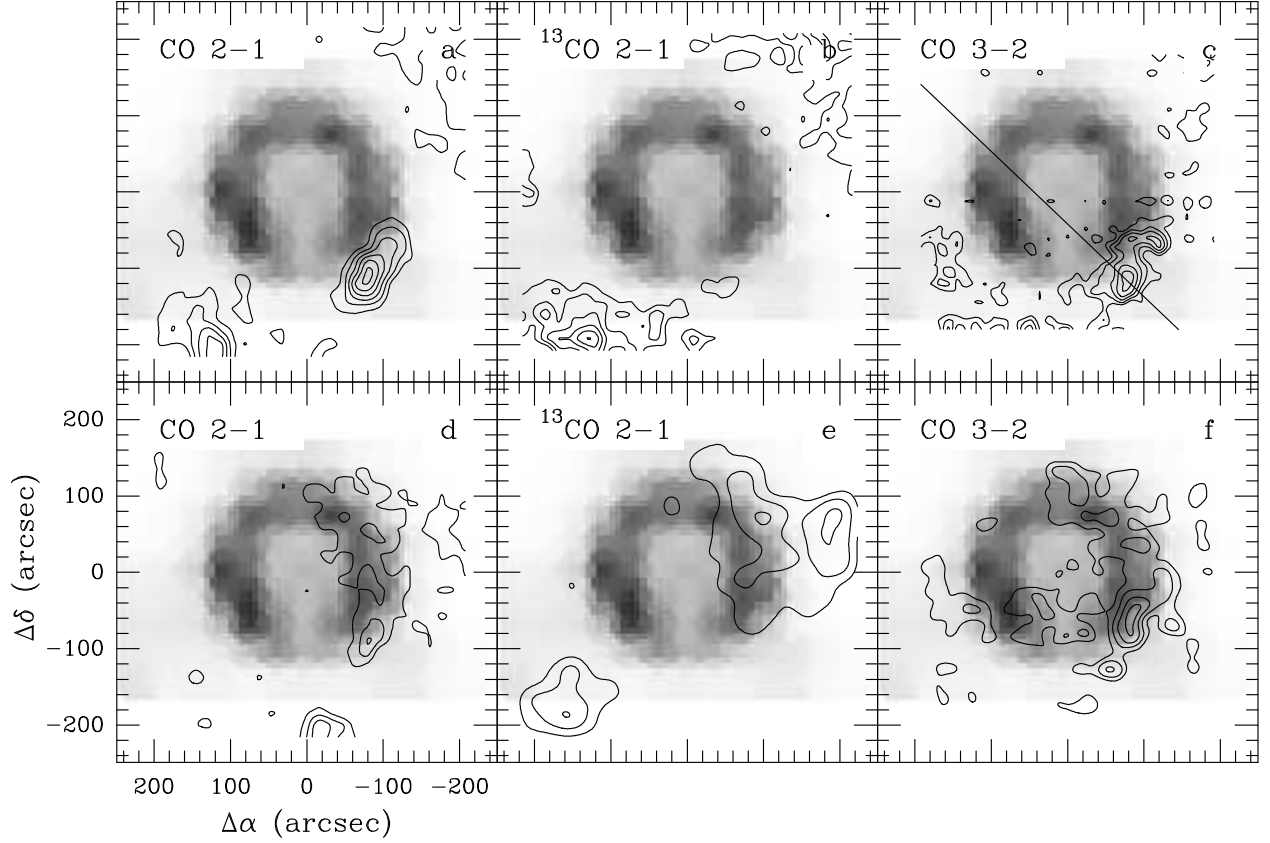


Fig. 4.— Background-removed maps of the three lines observed, integrated in two different velocity ranges: from 1.3 to 4.8 km s^{-1} (panels **a** to **c**), and from -3.0 to -1.3 km s^{-1} (panels **d** to **f**). Lines are indicated at the top left of each map. Contours are overlaid to an ISO $25\mu\text{m}$ image of the nebula (Trams et al. 1997). Contours start and spacing are 1.6, 1.0, 4.4, 1.0, 0.4, and 1.0 K km s^{-1} from **a** to **f**, respectively. The diagonal line on map **c** marks the strip selected for the position-velocity diagram shown in Fig. 5

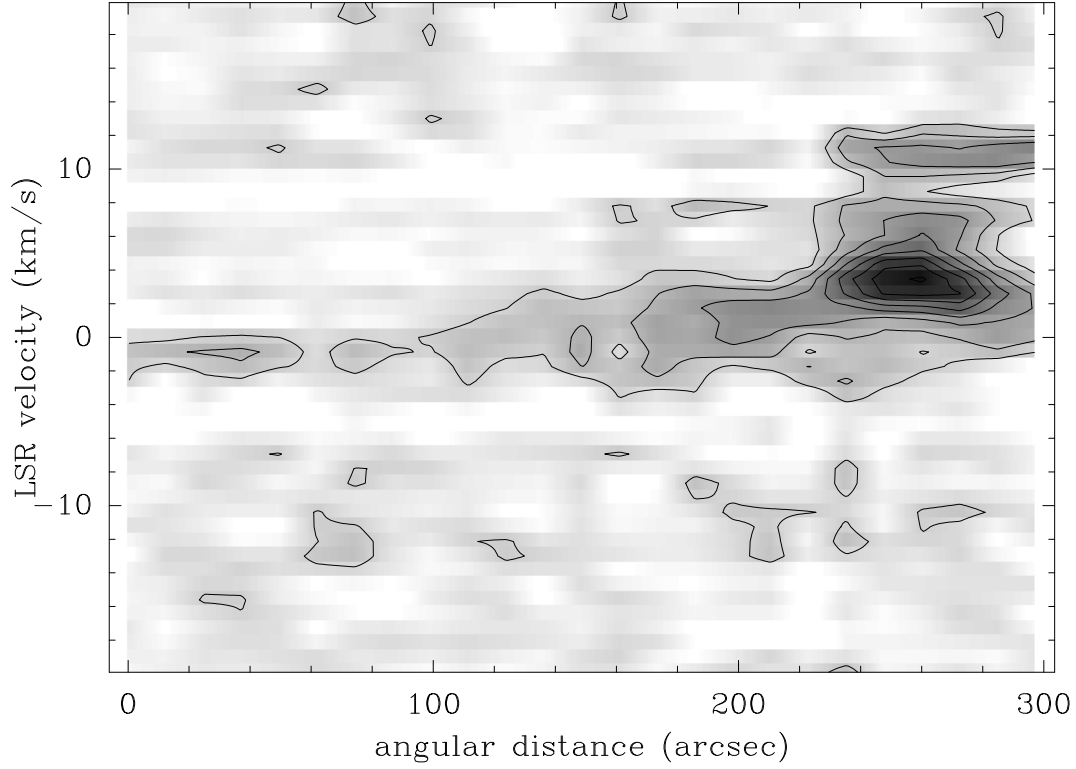


Fig. 5.— Position-velocity diagram of the CO $J = 3 \rightarrow 2$ line emission in the field of G79.29+0.46. The direction of the slice is traced by the line in Fig. 4c, oriented 45° from northeast to southwest. The notable broadening near $260''$ corresponds to the southwest arc just beyond the nebula (see text)

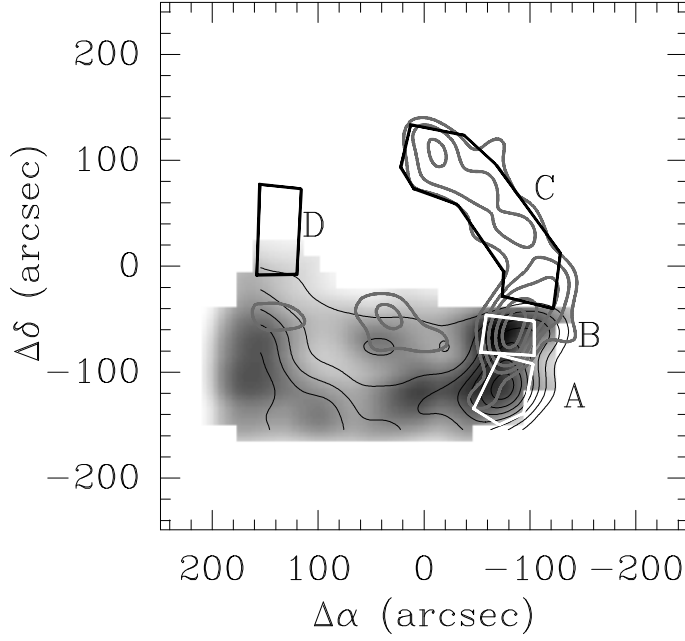


Fig. 6.— Regions selected for the LVG modelling, indicated by letters A, B, C and D. Greyscale corresponds to the CO $J = 3 \rightarrow 2$ to $2 \rightarrow 1$ line ratio (R_{exc}) in the velocity interval $(+1.3, +4.8)$ km s $^{-1}$. Black, thin contours correspond to the CO $J = 3 \rightarrow 2$ line emission in the same velocity interval. Grey, heavy contours trace the same but in the velocity interval $(-3, -1.3)$ km s $^{-1}$. All data have been convolved to $36''$ of angular resolution